





THE AUTOMATED DISCOVERY OF KINETIC RATE MODELS - METHODOLOGICAL FRAMEWORKS


A PREPRINT


 **Miguel Ángel de Carvalho Servia**
Department of Chemical Engineering
Imperial College London
South Kensington, London, SW7 2AZ, UK
m.de-carvalho-servia21@imperial.ac.uk

 **Ilya Orson Sandoval**
Department of Chemical Engineering
Imperial College London
South Kensington, London, SW7 2AZ, UK
o.sandoval-cardenas20@imperial.ac.uk

 **Klaus Hellgardt**
Department of Chemical Engineering
Imperial College London
South Kensington, London, SW7 2AZ, UK
k.hellgardt@imperial.ac.uk

 **King Kuok (Mimi) Hii**
Department of Chemistry
Imperial College London
White City, London, W12 0BZ, UK
mimi.hii@imperial.ac.uk

 **Dongda Zhang ***
Department of Chemical Engineering
The University of Manchester
Manchester, M13 9PL, UK
dongda.zhang@manchester.ac.uk

 **Ehecatl Antonio del Rio Chanona ***
Department of Chemical Engineering
Imperial College London
South Kensington, London, SW7 2AZ, UK
a.del-rio-chanona@imperial.ac.uk

January 30, 2023

ABSTRACT

The industrialization of catalytic processes is of far more importance today than it has ever been before and kinetic models are essential tools for their industrialization. Kinetic models affect the design, the optimization and the control of catalytic processes, but they are not easy to obtain. Classical paradigms, such as mechanistic modeling require substantial domain knowledge, while data-driven and hybrid modeling lack interpretability. Consequently, a different approach called automated knowledge discovery has recently gained popularity. Many methods under this paradigm have been developed, where ALAMO, SINDy and genetic programming are notable examples. However, these methods suffer from important drawbacks: they require assumptions about model structures, scale poorly, lack robust and well-founded model selection routines, and they are sensitive to noise. To overcome these challenges, the present work constructs two methodological frameworks, Automated Discovery of Kinetics using a Strong/Weak formulation of symbolic regression, ADoK-S and ADoK-W, for the automated generation of catalytic kinetic models. We leverage genetic programming for model generation, a sequential optimization routine for model refinement, and a robust criterion for model selection. Both frameworks are tested against three computational case studies of increasing complexity. We showcase their ability to retrieve the underlying kinetic rate model with a limited amount of noisy data from the catalytic system, indicating a strong potential for chemical reaction engineering applications.

Keywords: chemical reaction engineering, kinetic model generation, automated knowledge discovery, information criteria, machine learning

1 Introduction

Mathematical models are simplified descriptions of complex phenomena using a logic-based language. These models are widely used in science and engineering, be it in physics to represent human mobility patterns Song et al. [2010], Brockmann et al. [2006], in medicine to represent the metastatic spread of cancer Franssen et al. [2019], Margarit and Romanelli [2016], or in chemical reaction engineering to represent the reaction kinetics of a specific process Schbib et al. [1996], Battiston et al. [1982]. The wide usage of mathematical models across disciplines and fields is a direct consequence of their high utility, both fundamentally and practically. Fundamentally, these models allow researchers to simplify and distill complicated phenomena to quantitative mathematical expressions. Practically, they allow engineers to develop industrial processes and researchers to investigate the kinetics of a chemical system.

Given the importance of models, it is imperative to answer: how can models be constructed? Classically, this construction can be divided into three distinct paradigms: mechanistic, data-driven and hybrid modeling. Mechanistic models (also referred to as white-box models) are constructed and derived purely using existing fundamental laws, such as conservation equations and constitutive relations Baker et al. [2018]. Hypotheses are frequently made during the construction of a mechanistic model with the trade-off between accuracy and simplicity in mind. These hypotheses are usually manifested through equations of state, or empirical expressions Gernaey [2015]. Mechanistic models have a great number of advantages, such as: being derived from prior expert knowledge, the parameters being physically meaningful, having great extrapolatory properties, and being interpretable. For these reasons, these models are still widely established in industry. Nevertheless, some of these advantages are double-edged swords. For example, to construct these models via existing fundamental laws, a modeler must have strong background knowledge, the construction is usually time-consuming, the level of nonlinearity may be high, and if the process is not perfectly understood a mechanistic model may be infeasible. Also, having complicated nonlinear models results in increased experimental effort to collect sufficient data for the estimation of parameters.

Whereas mechanistic models technically may not require data for their structure identification (they may still require data for parameter estimation and validation), data-driven models solely use data for their construction. Unlike mechanistic models, data-driven models can be designed relatively quickly, and their construction requires no knowledge about the system being investigated. Their structure is highly flexible, and can be promptly repurposed to account for more variables or to describe different processes. Data-driven approaches are also generally quicker to evaluate than mechanistic ones, and as a result of this, the former have a lot of potential in real-time simulation Zhang et al. [2019], del Rio-Chanona et al. [2018a], Park et al. [2021], Sun et al. [2022], optimization Petsagkourakis et al. [2020], del Rio-Chanona et al. [2018b], Wu et al. [2023], Natarajan et al. [2021], and soft sensor development Mowbray et al. [2022a], Kay et al. [2022], Kadlec et al. [2009]. However, since no physical knowledge is used to make the black-box models, their prediction tends to be poor outside the range of data used to train them (i.e.: poor extrapolatory abilities), which might classify their usage in certain scenarios as unsafe. Their performance is highly influenced by the quantity and quality of data available, and data pre-treatment before training a model is frequently required.

The last class of models are the hybrid models. This type of models attempts to exploit the best of mechanistic and data-driven modeling. In its essence, a hybrid model has a mechanistic backbone and a data-driven block which tries to improve the fit of the backbone. There are two main approaches to hybrid modeling: parallel and sequential. In the parallel approach, the data-driven block describes the model-data mismatch. In the sequential approach, the data-driven block describes one or more parameters of the mechanistic backbone that may be dependent on multiple variables. Or, the mechanistic backbone is integrated within the data-driven architecture. In either approach, generally, the hybrid model will retain the extrapolation capabilities of a mechanistic model, whilst retain the flexibility and ease of construction of a data-driven model Vega-Ramon et al. [2021], Mowbray et al. [2022b], Zhang et al. [2020].

At face value, hybrid modeling seems like an elegant solution to the problems posed by mechanistic and data-driven modeling, albeit not the only one. Another effective solution is to utilize existing data to automatically generate and select mechanistic models by exploiting state-of-the-art statistical and machine learning methods. In this way, the benefits of mechanistic models are maintained (e.g.: extrapolatory abilities, interpretability and physical meaning), whilst some of their drawbacks are eliminated (e.g.: needing background knowledge, expensive and time-consuming). This strategy/paradigm has been (loosely) named *automated knowledge discovery*. Formally, it is known as symbolic regression Haider et al. [2023]. The methodology presented in this work follows this paradigm.

Before going further we will set the mathematical notation that is shared between both optimization approaches. We set a predefined time interval $\Delta t = [t_0, t_f]$ and denote the state variables as $x(t) \in \mathbb{R}^{n_x}$. The input dataset consists of pairs (t_i, y_i) for a given set \mathcal{T} of n_t sampling times t_i , where $t_i \in \Delta t$ and $y_i \in \mathbb{R}^{n_t}$. \mathcal{M} is the set of symbolic expressions reachable by the search procedure, where each model $m \in \mathcal{M}$ has a finite set of tunable parameters θ_m whose dimension depends on each proposed model: $m(\cdot, \theta_m)$. The predicted state variables are denoted by $\hat{x}(t)$, and $L(\hat{x}(t), y(t))$ is the discrepancy measure between our predictions and the measured values, which characterizes the performance of the model (e.g.: least squares function, likelihood function).

Symbolic regression, in its strong formulation, aims to find the model that best maps the time to the state variables directly:

$$\hat{x}_m(t, \theta_m) = m(t, \theta_m). \quad (1)$$

In its weak formulation, it aims to find the model that best maps input variables to output variables as a differential equation system:

$$\dot{x}(t, \theta_m) = m(x(t), \theta_m) \quad (2a)$$

$$\hat{x}_m(t, \theta_m) = \int_{t_0}^t \dot{x}(\tau, \theta_m) d\tau \quad (2b)$$

The optimization problem for both formulations can be expressed as follows:

$$m^*(t, \theta_m^*) = \min_{m \in \mathcal{M}, \theta_m} \sum_{t_i \in \mathcal{T}} L(\hat{x}_m(t_i, \theta_m), y_i). \quad (3)$$

A wide variety of methods have been proposed in literature to solve the symbolic regression problem. These include but are not limited to: the ALAMO approach Wilson and Sahinidis [2017], the SINDy algorithm Brunton et al. [2016], the work by Taylor and colleagues Taylor et al. [2021], the work by Neumann and colleagues Neumann et al. [2020], and genetic programming Koza [1994]. Popular automated knowledge discovery frameworks frequently face at least one of four challenges that may limit their ability to retrieve underlying ground-truth models, and consequently, their real-world applicability. Firstly, they necessitate structural assumptions of the underlying data-generating model. This is particularly true for some non-evolutionary strategies, as a design matrix (i.e.: a model library) needs to be constructed for their execution Wilson and Sahinidis [2017], Brunton et al. [2016]. Secondly, they may display poor scalability with respect to the number of state variables available (this is also particularly true of non-evolutionary strategies) Wilson and Sahinidis [2017], Brunton et al. [2016], Taylor et al. [2021], Neumann et al. [2020]. Thirdly, they lack a motivated and rigorous model selection routine (i.e.: their choice of model selection routine may not be transparent and/or different routines are not tested) Wilson and Sahinidis [2017], Brunton et al. [2016], Taylor et al. [2021], Neumann et al. [2020], Koza [1994]. Lastly, for the discovery of non-linear dynamics, they may be sensitive to noisy data when rate measurements are not directly accessible Wilson and Sahinidis [2017], Brunton et al. [2016], Taylor et al. [2021], Neumann et al. [2020], Koza [1994].

In this section, we introduced the importance of mathematical modeling within chemical engineering, the challenges of classical modeling paradigms, and the shortcomings of modern automated knowledge discovery methodologies. This work aims to construct two generalizable and robust methodological frameworks that integrate a rigorous model selection routine for the automated kinetic rate model discovery. The rest of the paper is organized as follows: in Section 2 two proposed methods are motivated and described in detail; in Section 3 we introduce three case studies that are used to analyze the performance of the proposed methodological frameworks; in Section 4 the results of the study are presented and amply discussed along with the shortcomings of the proposed methodologies; and in Section 5 the key findings are presented with a brief outlook on future research.

2 Methodological Frameworks

The two proposed methodological frameworks are comprised of three stages: model generation, model refinement and model selection. In this section we expand on each of these steps and present the distinctive characteristic of each of the proposed frameworks.

Genetic programming (GP) is often considered one of the most generalizable and reliable model generation methods

found in literature for an important reason: the flexibility to include prior knowledge. Its execution requires minimal assumptions about the ground-truth model. As a direct contrast to ALAMO (note: ALAMO is formulated as a cardinality constrained mixed-integer quadratic program, or more simply, as a mixed integer non-linear program) and SINDy (note: SINDy was initially formulated as non-linear program, however, SINDy can also be solved via mixed-integer optimization Bertsimas and Gurnee [2022]), GP does not need a design matrix. However, if knowledge about the ground-truth model is available (e.g.: mass and energy balances), this can be provided via mathematical constraints alike ALAMO and SINDy.

A especially attractive quality of GP when compared to mixed-integer based alternatives is the explicit control over the levels of complexity in the resulting expressions. The generalization of a model has a close relationship with the complexity of it in relation to the available data. Approaches based on a design matrix, which mixes expressions of multiple complexities, does not control the resulting expression complexity, instead it controls the cardinality. An explicit report of several expressions of increasing complexity provides more value to the modeler in order to commit with one of the proposals. Here, complexity refers to the sum of all terms of a particular function. For instance, $f(x) = \frac{x^2+2x-4}{5x}$ would have a complexity equal to 13, since each operator, constant and variable count as 1. As such, we propose that GP should be used for the kinetic rate model generation stage of both frameworks.

The basic concept of GP is to specify a set of state variables (e.g.: temperature, pressure, concentration) and operators (e.g.: '+', '/') that may be present in the underlying mechanistic model. This selection can be as relaxed or constrained as the modeler decides. User-defined analytical functions (e.g.: $\frac{1}{k_1x_1+k_2x_2}$) may also be specified to be included within generated models. With this, an initial population of models can be constructed. Quoting Darwin’s theory of evolution, the best models — based on a specified performance metric — are evolved via genetic operations (e.g.: crossover and mutation), and the worst models are discarded. This process is iterated until convergence is achieved or a termination criterion is met.

By virtue of GP, model parameters are stochastically evolved through genetic mutations, using differential evolution, and not by explicitly solving a parameter estimation problem. As such, a model refinement stage is needed as a parameter estimation problem, where the error between the model’s response and the data are minimized by finding the best set of kinetic parameters.

In GP, the most accurate generated model for each complexity level is output (the upper bound of complexity is user-defined). Therefore, a model selection stage is needed to discern which kinetic rate model proposed is the most appropriate for a particular dataset.

2.1 Introduction to ADoK-S

The first proposed methodological framework, ADoK-S (Automated Discovery of Kinetics using a Strong formulation of symbolic regression), uses GP to solve the strong formulation of the symbolic regression to find kinetic rate models. A characteristic of the strong formulation of symbolic regression is that only models that can directly map the specified state variables to the output variable are proposed. Therefore, in the context of kinetic rate model discovery, rate measurements need to be provided to find the desired model; rate is defined as:

$$r = \frac{1}{\nu_i} \frac{dC_i}{dt} \quad (4)$$

where ν_i and $\frac{dC_i}{dt}$ represent the stoichiometric coefficient and the rate of change of concentration with respect to time of species i , respectively.

Realistically, seldom does a modeler have direct access to rate measurements, and therefore it would be practically meaningless to assume that these measurements are indeed available. Classically, to construct a mechanistic kinetic rate model of a chemical system, a modeler only has access to discrete measurements of the concentration of observed species with respect to time (for batch reactors) or with respect to residence time (for continuous plug flow reactors). With this dataset, assumptions about the kinetics of the system are made (e.g.: first order or second order kinetics), models are generated, kinetic parameters are estimated by using the dynamic trajectories of the concentrations, and a final model is proposed. Thus, it is fair to assume that concentration data with respect to time are available to a modeler.

Under the assumption that dynamic trajectories of concentrations are available, and knowing that the strong formulation of symbolic regression requires rate measurements of the chemical reaction, it is evident that these measurements must be estimated from the available data. Assuming an isochoric and isothermal system, it can be claimed that C_i (the concentration of species $i \in \mathbb{Z}^+$) is only dependent on time. Mathematically, under these conditions, the concentration profile of an arbitrary species is a function only dependent on time, $C_i = f_i(t)$. Therefore, if $f_i(t)$ can be accurately estimated, discrete rate measurements can also be estimated by numerically differentiating the concentration profile. To avoid limiting assumptions, GP is used to estimate $f_i(t)$, as output measurements C_i and input measurements t are available.

Finding an appropriate concentration profile follows the three stages referred earlier: model generation, model refinement, and model selection. For the model generation stage, an implementation of GP done by Cranmer and colleagues was used Cranmer [2020]. For the model refinement stage, posed as a parameter estimation problem, the error between a model’s response and the data are minimized by finding the best set of kinetic parameters. This optimization problem is solved by carrying out an initial screening of the kinetic parameter search space using the artificial bee colony (ABC) algorithm. The best output from the ABC is used to warm-start the limited-memory Broyden-Fletcher-Goldfarb-Shanno (LBFGS) algorithm. The ABC algorithm was chosen because of its excellent explorative characteristics Cho et al. [2021]. Whereas, the LBFGS algorithm was chosen because of its excellent performance in the parameter estimation task Malouf [2002], and optimization in general Liu and Nocedal [1989]. The objective function used for the parameter estimation in this work was the negative log-likelihood (NLL), presented below:

$$\text{NLL}(\theta) = \sum_{i,j,k} \left[\frac{(C_{i,j,k} - y(\theta)_{i,j,k})^2}{2\hat{\sigma}_i^2} - \log \left(\frac{1}{\sqrt{2\pi\hat{\sigma}_i^2}} \right) \right] \quad (5)$$

where $C_{i,j,k}$ is the measured concentration (i.e.: in-silico data) of species $i \in S$ for dataset $j \in D$ at time $k \in T$, where S , D , and T represent the species set, data set and time set, respectively; $y(\theta)_{i,j,k}$ is the concentration of species $i \in S$ for dataset $j \in D$ at time $k \in T$ proposed by an arbitrary model which is dependent on its parameters θ ; $\hat{\sigma}_i^2$ is the variance of the noise that we assume the concentrations of species $i \in S$ have.

For the model selection stage, the Akaike information criterion (AIC) is used to determine which model is the best ones. The AIC was selected after a thorough analysis of the performance of different criteria (finite-sampled corrected AIC, Bayesian information criteria and Hannan Quinn criterion) under several conditions (e.g.: different amounts of additive noise, different amounts of data). This analysis concluded that AIC has a higher probability of selecting the correct data-generating rate model than the other criteria tested. The AIC selects the model which has the lowest AIC value calculated from the below expression:

$$\text{AIC}_m = 2\text{NLL}(\theta)_m + 2d_m \quad (6)$$

here the subscript m serves to represent model $m \in M$, where M is the set of proposed models; d_m represents the number of parameters present in a model $m \in M$.

Once a concentration model has been successfully generated, refined and selected, this same model $C_i = f_i(t)$ is numerically differentiated using the central difference method. In this way, a new training dataset is generated, where the inputs are the discrete measurements of concentration through time and the outputs are the discrete estimates of the rate measurements through time. Given that the rate is a function of the concentration of the species ($r = f(C_1, C_2, \dots)$), the same protocol outlined above can be executed again with the new training dataset. By doing so, rate models that take as inputs the concentrations of the species observed in the chemical system and outputs the rate of that same system are generated using GP. Then, using the ABC and the LBFGS algorithms, the models are refined; using AIC, the best model is selected.

Once an optimized kinetic rate model is selected by AIC, this model is numerically integrated using the LSODA algorithm Hindmarsh and Petzold [2005] ($\int r dt = \int \frac{1}{\nu_i} \frac{dC_i}{dt} dt = \frac{1}{\nu_i} C_i(t)$) implemented in SciPy python package Virtanen et al. [2020]. The results from this integration are directly compared to the original datasets of the dynamical trajectories of the observed concentrations. If the results are satisfactory to the modeler, the methodological framework

is terminated. Otherwise, further data should be collected by applying (model-based) design of experiments. For the sake of clarity and simplicity, the flowchart of the proposed methodological framework is presented in Figure 1.

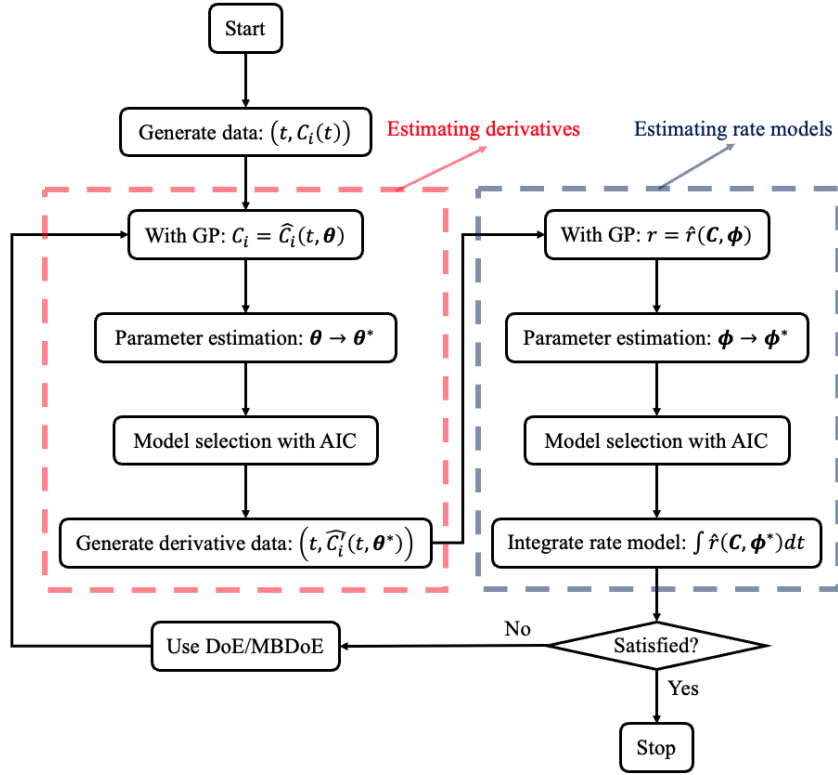


Figure 1: The flowchart of ADoK-S (Automated Discovery of Kinetics using a Strong formulation of symbolic regression); the red and blue dashed boxes represent the steps where rate measurements and rate models are estimated, respectively.

2.2 Introduction to ADoK-W

One of the primary reasons to solve the symbolic regression problem is to retrieve interpretable mathematical expressions that experts can analyze and validate. But perhaps more importantly, expressions that experts can extract knowledge from them. Clearly, the strong formulation of symbolic regression hinders this process within the catalytic reaction engineering context. As explained in the previous section, to successfully implement the strong formulation of symbolic regression, ADoK-S must first propose and refine concentration profiles, where the best one (selected by AIC) is used to estimate rate measurements. Catalytic reaction engineers seldom know the model structure of a concentration profile, especially because many kinetic rate models do not have a close-form solution. As such, experts would find the task to validate concentration models strenuous, perhaps even impossible. Furthermore, having a model that describes the dependence of the concentration of a species with respect to time does not provide significant and actionable information to the experts. In other words, experts cannot extract much knowledge from these models and we can conclude that the strong formulation of symbolic regression inevitably affects the interpretability of ADoK-S.

The strong formulation of symbolic regression may also affect the performance of ADoK-S with regards to noisy data. The necessity to have the first step of ADoK-S is that rate measurements are required to retrieve a kinetic rate model (as the strong formulation only allows the direct mapping of inputs to outputs). As previously mentioned, having direct access to the rate measurements of a dynamical catalytic chemical system is a rarity and thus need to be estimated. As it is explained in Bertsimas and Gurnee [2022], numerical differentiation exacerbates any noise inherent to the measured data, and even robust differentiation techniques (e.g.: polynomial interpolation) may not be enough to provide usable derivative data. In ADoK-S, these effects are minimized by selecting a concentration profile model with the AIC, but the effects are not eradicated. Therefore, we can conclude that the strong formulation of symbolic regression may also

affect the performance of ADoK-S.

The innate drawbacks of the strong formulation for the automated kinetic rate discovery task motivated the construction of a different methodological framework. ADoK-W (Automated Discovery of Kinetics using a Weak formulation of symbolic regression) aims to combine the two steps from the previous framework into a single one by reformulating the symbolic regression problem. The weak reformulation of symbolic regression bypasses altogether the construction of concentration profile models, and the subsequent numerical differentiation to obtain estimations of the rate measurements. Whereas the strong formulation provides a direct mapping between inputs and outputs, the weak formulation of symbolic regression represents a mapping between input and output variables in the derivative space. In other words, this reformulation generates models dependent on the state variables that can map the output via an integration step. In this way, the GP algorithm receives the dynamic trajectories of concentration as inputs, proposes rate models ($r = f(C_1, C_2, \dots)$ where C_i is the concentration of species $i \in \mathbb{Z}^+$), integrates the rate models with respect to time at each given time-step where concentration data is available ($\int r dt = \int \frac{1}{\nu_i} \frac{dC_i}{dt} dt = \frac{1}{\nu_i} (C_i(t=t) - C_i(t=0))$), and compares the results from the integration with the original dataset.

Similarly to ADoK-S, due to the usage of a GP algorithm to solve the symbolic regression problem, the proposed rate models may have under-evolved kinetic parameters and therefore necessitate a model refinement stage. As explained in the previous section, this model refinement stage is posed as a parameter estimation problem, where Equation 5 is used as the objective function. To solve this problem, the kinetic parameter search space is initially scanned by the ABC algorithm, where its output is used as a warm-start for the LBFGS algorithm which will output the final set of kinetic parameters. If desirable, this optimization routine can be repeated multiple times to improve the probability of reaching a global optimum. Then, alike ADoK-S, the best model is selected based on the AIC value produced from Equation 6.

In identical fashion to the previously presented methodological framework, once an optimized kinetic rate model is selected by AIC, this model is numerically integrated using the LSODA algorithm. The results from this integration are directly compared to the original datasets of the dynamical trajectories of the observed concentrations. If the results are satisfactory to the modeler, the methodological framework is terminated. Otherwise, further data should be collected by applying (model-based) design of experiments. For the sake of clarity and simplicity, the flowchart of the proposed methodological framework is presented in Figure 2.

3 Catalytic Kinetic Case Studies

To showcase the performance of the proposed methodological frameworks, three illustrative catalytic kinetic case studies were chosen: an isomerization reaction, the decomposition of nitrous oxide, and the toluene hydrodealkylation. Below, their respective kinetic rate models are introduced, along with how the required datasets (i.e.: dynamic trajectories of concentrations) are generated.

3.1 Isomerization Reaction

The simplest case study presented in this work is a catalytic isomerization reaction, where A is transformed to B reversibly over a catalytic active site. The reaction is shown below.



The kinetic rate model that describes the evolution of the concentrations of A and B through time is shown below. This expression has been directly borrowed from the book by Marin and colleagues Marin et al. [2019].

$$r = -\frac{dC_A}{dt} = \frac{dC_B}{dt} = \frac{k_A C_A - k_B C_B}{k_C C_A + k_D C_B + k_E} \quad (8)$$

In Equation 8, C_A and C_B represent the concentration of reactant A and product B , respectively. The kinetic parameters of the kinetic rate model are represented by k_i where $i \in [A, B, \dots, E]$. To generate the necessary dataset to test both frameworks, three computational experiments are carried out, each with different initial conditions. The computational experiments are run with the following initial conditions (in molar units, mol L⁻¹): $(C_{A,0}, C_{B,0}) \in \{(2, 0), (6, 1), (10, 2)\}$. For each computational experiment, the concentration of the reactant and

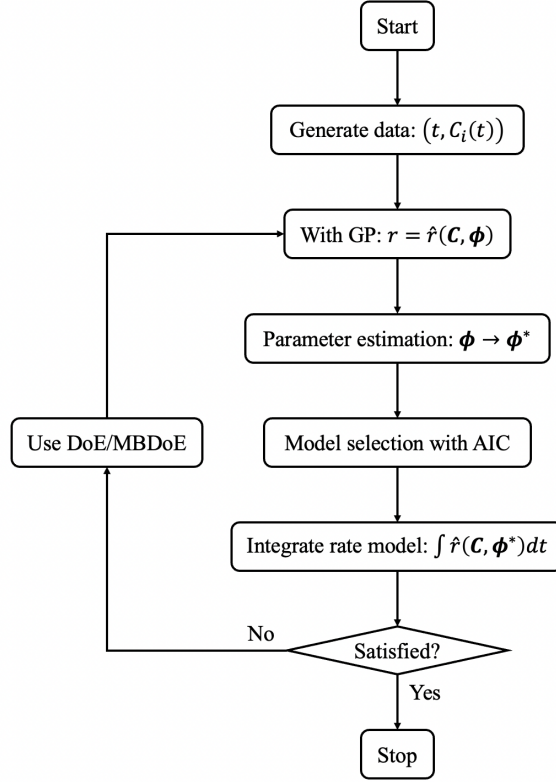


Figure 2: The flowchart of ADoK-W (Automated Discovery of Kinetics using a Weak formulation of symbolic regression).

product are recorded 10 times, at evenly spaced intervals between time $t=0$ s and $t=10$ s. For this particular case study, the kinetic parameters were defined as: $k_A=7 \text{ M s}^{-2}$, $k_B=3 \text{ M s}^{-2}$, $k_C=4 \text{ s}^{-1}$, $k_D=2 \text{ s}^{-1}$ and $k_E=6 \text{ M s}^{-1}$.

To approximate the behavior of a realistic chemical system, Gaussian noise was added to the computational experimental measurements, yielding the needed dynamic trajectories of concentrations. The defined Gaussian noise has zero mean and a standard deviation of 0.17 for the concentrations of A , and 0.18 for the concentrations of B (the standard deviations represent 5% of the mean of the concentrations of A and B). For the parameter estimation task, it would be futile to assume that, as modelers, the exact variance of the noise would be known. Thus, a conservative assumption is made by setting $\hat{\sigma}_A=0.35$ and $\hat{\sigma}_B=0.35$ (i.e.: assuming a standard deviation of 10% of the mean of the concentrations of A and B). The generated data of one of the computational experiments are presented in Figure 3. All the graphs presented in this paper have been generated using the Matplotlib package implemented in Python Hunter [2007].

3.2 Decomposition of Nitrous Oxide

The second case study presented in this work is the catalytic decomposition of nitrous oxide, where nitrous oxide (N_2O) is transformed to nitrogen gas (N_2) and oxygen gas (O_2). The reaction is shown below.



The kinetic rate model that describes the evolution of the concentrations of N_2O , N_2 and O_2 through time is shown below. This expression has been directly borrowed from the book by Levenspiel [1998].

$$r = -2 \frac{dC_{\text{N}_2\text{O}}}{dt} = 2 \frac{dC_{\text{N}_2}}{dt} = \frac{dC_{\text{O}_2}}{dt} = \frac{k_A C_{\text{N}_2\text{O}}^2}{1 + k_B C_{\text{N}_2\text{O}}} \quad (10)$$

In Equation 10, C_{N_2O} , C_{N_2} and C_{O_2} represent the concentration of reactant nitrous oxide, and of products nitrogen gas and oxygen gas, respectively. The kinetic parameters of the kinetic rate model are represented by k_i where $i \in [A, B]$. To generate the necessary dataset to test both frameworks, three computational experiments are carried out, each with different initial conditions. The experiments are run with the following initial conditions (in molar units): $(C_{N_2O,0}, C_{N_2,0}, C_{O_2,0}) \in \{(5, 0, 1), (7.5, 1, 2), (10, 2, 3)\}$. For each experiment, the concentration of the reactant and products are recorded 10 times, at evenly spaced intervals between time $t=0$ s and $t=10$ s. For this particular case study, the kinetic parameters were defined as: $k_A=2 \text{ M}^{-1} \text{ s}^{-1}$ and $k_B=5 \text{ M}^{-1}$.

To approximate the behavior of a realistic chemical system, Gaussian noise was added to the in-silico datasets, yielding the needed dynamic trajectories of concentrations. The defined Gaussian noise has zero mean and a standard deviation of 0.11 for the concentrations of N_2O , 0.32 for the concentrations of N_2 , and 0.23 for the concentration of O_2 (the standard deviations represent 5% of the mean of the concentrations of N_2O , N_2 and O_2). For the parameter estimation task, it would be futile to assume that, as modelers, the exact variance of the noise would be known. Thus, a conservative assumption is made by setting $\hat{\sigma}_{N_2O}=0.22$, $\hat{\sigma}_{N_2}=0.63$ and $\hat{\sigma}_{O_2}=0.46$ (i.e.: assuming a standard deviation of 10% of the mean of the concentrations of N_2O , N_2 and O_2). The generated data of one of the computational experiments are presented in Figure 3.

3.3 Toluene Hydrodealkylation

The third and most complex case study (i.e.: case study with most species involved in the chemical reaction) presented in this work is the catalytic toluene hydrodealkylation to benzene, where toluene ($C_6H_5CH_3$) and hydrogen gas (H_2) is transformed to benzene (C_6H_6) and methane (CH_4). The reaction is shown below.



The kinetic rate model that describes the evolution of the concentrations of $C_6H_5CH_3$, H_2 , C_6H_6 and CH_4 through time is shown below. This expression has been directly borrowed from the book by Fogler [2016].

$$r = -\frac{dC_T}{dt} = -\frac{dC_H}{dt} = \frac{dC_B}{dt} = \frac{dC_M}{dt} = \frac{k_A C_T C_H}{1 + k_B C_B + k_C C_T} \quad (12)$$

In Equation 12, C_T , C_H , C_B and C_M represent the concentration of reactants toluene and hydrogen, and of products benzene and methane, respectively. The kinetic parameters of the kinetic rate model are represented by k_i where $i \in [A, B, C]$. To generate the necessary dataset to test both frameworks, three computational experiments are carried out, each with different initial conditions. The computational experiments are run with the following initial conditions (in molar units): $(C_{T,0}, C_{H,0}, C_{B,0}, C_{M,0}) \in \{(1, 3, 0, 0.5), (3, 5.5, 1, 1.75), (5, 8, 2, 3)\}$. For this particular case study, for each experiment, the concentration of the reactant and products are recorded 50 times, at evenly spaced intervals between time $t=0$ s and $t=10$ s. The frequency of the sampling was increased due to the complexity of the case study. It should be noted that this increment is still within the realistic range of experimental sampling frequency, as these samples could have been gathered from a continuous-flow experiment Schrecker et al. [2023]. The kinetic parameters were defined as: $k_A=2 \text{ M}^{-1} \text{ s}^{-1}$, $k_B=9 \text{ M}^{-1}$ and $k_C=5 \text{ M}^{-1}$. It should be noted that, for each of the case studies, only the model structure is borrowed from literature. The value of the kinetic parameters are randomly assigned.

To approximate the behavior of a realistic chemical system, Gaussian noise was added to the experimental results, yielding the needed dynamic trajectories of concentrations. The defined Gaussian noise has zero mean and a standard deviation of 0.09 for the concentrations of toluene, 0.16 for the concentrations of hydrogen gas, 0.07 for the concentration of benzene, and 0.15 for the concentration of methane (the standard deviations represent 5% of the mean of the measured concentrations of toluene, hydrogen gas, benzene and methane). For the parameter estimation task, same as before, a conservative assumption is made by setting $\hat{\sigma}_T=0.18$, $\hat{\sigma}_H=0.33$, $\hat{\sigma}_B=0.14$, and $\hat{\sigma}_M=0.30$ (i.e.: assuming a standard deviation of 10% of the mean of the concentrations of toluene, hydrogen gas, benzene and methane). The generated results of one of the computational experiments are presented in Figure 3.

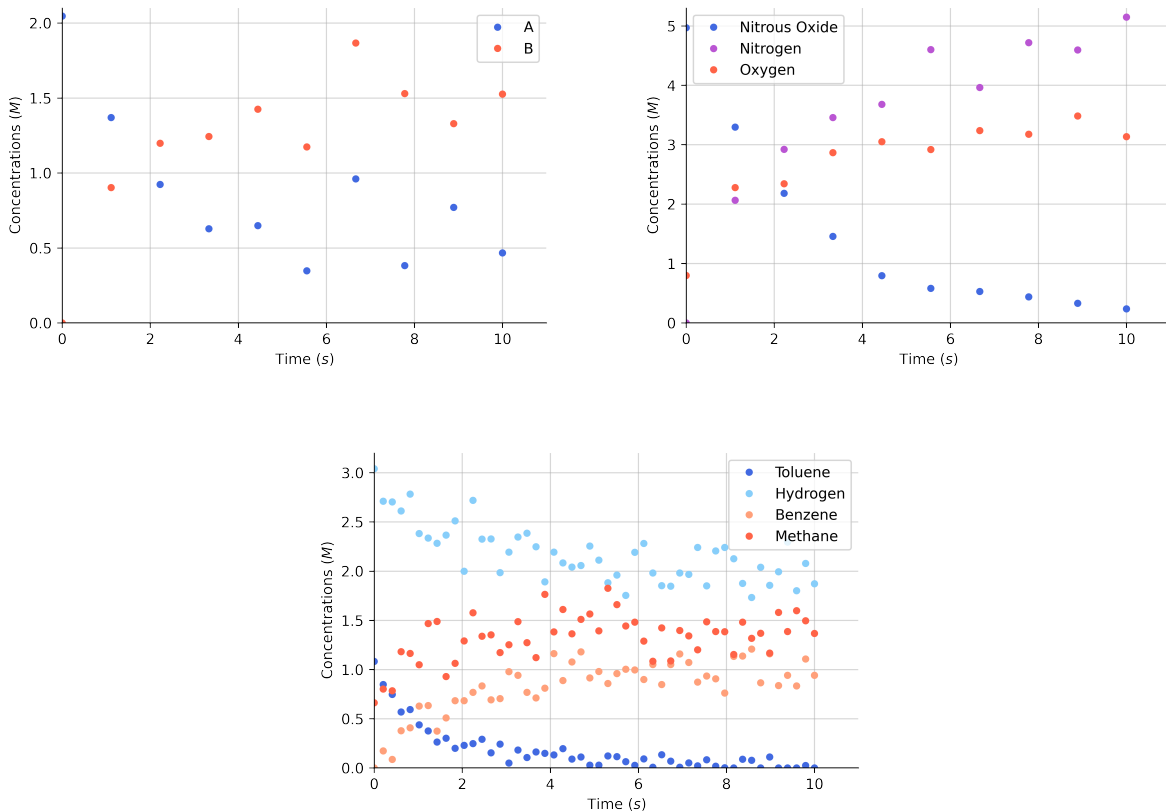


Figure 3: Top left: The in-silico data of one of the computational experiments for the catalytic isomerisation reaction. Top right: The generated data of one of the computational experiments for the catalytic decomposition of nitrous oxide reaction. Bottom: The generated data of one of the computational experiments for the catalytic hydrodealkylation of toluene reaction.

4 Results and Discussions

4.1 Isomerization Reaction — ADoK-S

As explained in Section 2.1, ADoK-S aims to solve a strong formulation of symbolic regression by implementing GP. In this methodological framework, departing from the kinetic data generated (routine for data generation is detailed in Section 3), the GP algorithm is used to generate concentration profile models (i.e.: models which represent the evolution of concentration through time as a function of time, $f(t)$). The expression construction rules exclusively included the arithmetic operators '+', '-', '×', '/' and 'exp'. According to physical knowledge, this is a fair selection of operators as the likelihood of these operators appearing is extremely high (to the best of the author’s knowledge, trigonometric operators, for example, do not appear in concentration expressions). The generation of concentration profiles is carried out for reactant A and product B at each computational experiment (i.e.: 2 concentration models are generated for each experiment — $(f_{A,i}, f_{B,i})$ for $i \in [1, 2, 3]$). In a real case study, assuming that all of A gets transformed to B without forming any side-product would not be a valid assumption. For that reason, it would be bad practice to generate a model for the concentration of A (or B) and obtaining a model for B (or A) by simply solving the mass balance. As such, we must propose models for A and B separately to ensure that the rates are well predicted. Models must also be proposed for each experiment because, although the rate model is the same for each species, its integration is dependent on initial conditions. In other words, for different initial conditions, the concentration profiles have different functional forms. The same rational is applied to the subsequent case studies.

For the sake of brevity, only the results from the first experiment are presented, but the same routine is executed on all the other computational experiments. It is also specified that the proposed models should only include ' t ' as a variable. As explained in Section 2.1, the concentration profiles, assuming isochoric and isothermal conditions, should only be

dependent on time. The GP algorithm proposed the model structures for the concentration of A and B in experiment 1 shown below, where p_ℓ for $\ell \in [1, 2, 3, 4]$ are the parameters that can be estimated according to the concentration versus time dataset and $f_{i,j,k}$ refers to the k^{th} concentration model of species i in experiment j proposed by SR.

$$f_{A,1,1} = p_1 \quad (13a)$$

$$f_{A,1,2} = \exp(p_1 t) \quad (13b)$$

$$f_{A,1,3} = \frac{p_1}{t + p_2} \quad (13c)$$

$$f_{A,1,4} = \exp(p_1 - t) + p_2 \quad (13d)$$

$$f_{A,1,5} = p_1 + p_2 \exp(-p_3 t) \quad (13e)$$

$$f_{A,1,6} = \exp(-t)(p_1 t + p_2) + p_3 \quad (13f)$$

$$f_{A,1,7} = p_1 + \exp(-t) - \exp(-p_2 t) + p_3 \quad (13g)$$

$$f_{A,1,8} = \frac{p_1 t + p_2}{p_3 + \exp(t)} + p_4 \quad (13h)$$

$$f_{B,1,1} = p_1 \quad (14a)$$

$$f_{B,1,2} = \exp(p_1 t) \quad (14b)$$

$$f_{B,1,3} = p_1 + p_2 t \quad (14c)$$

$$f_{B,1,4} = p_1 - p_2 \exp(-t) \quad (14d)$$

$$f_{B,1,5} = p_1 - \frac{p_2}{t + p_3} \quad (14e)$$

$$f_{B,1,6} = p_1 - \frac{p_2}{p_3 + \exp(t)} \quad (14f)$$

$$f_{B,1,7} = \exp(-t)(p_1 t - p_2) + p_3 \quad (14g)$$

$$f_{B,1,8} = \frac{-p_1 t - p_2}{p_3 + \exp(t)} + p_4 \quad (14h)$$

For each of the proposed model structures shown above, parameter estimation is carried out by finding the parameters which minimizes Equation 5 (as mentioned, the assumed variances for NLL are double of the real variances used to generate the Gaussian noise). This problem is solved by employing the strategy outlined in Section 2.1 (i.e.: initial parameter screening with ABC algorithm and solution refinement with LBFGS algorithm).

Table 1 displays the NLL values along with the AIC values for each of the models, showing that $f_{A,1,4}$ is the best model for the concentration profile of A (in experiment 1), and showing that $f_{B,1,4}$ is the best model for the concentration profile of B (in experiment 1). We can conclude from the proposed concentration models that the catalytic system under investigation is not a complex one. This demonstrates that, although the first step of ADoK-S is mostly uninterpretable, it can still provide the modeler with some level of insightful information pertaining to the complexity of the system.

Table 1: The negative log likelihood values and the AIC values of all concentration profile models proposed by the GP algorithm for reactant A and product B for experiment 1.

Model	NLL Value	AIC Value	Model	NLL Value	AIC Value
$f_{A,1,1}$	9.285	20.570	$f_{B,1,1}$	7.764	17.528
$f_{A,1,2}$	4.175	10.351	$f_{B,1,2}$	5.126	12.252
$f_{A,1,3}$	-2.343	-0.686	$f_{B,1,3}$	3.726	11.451
$f_{A,1,4}$	-2.850	-1.701	$f_{B,1,4}$	2.079	8.159
$f_{A,1,5}$	-3.221	-0.442	$f_{B,1,5}$	1.897	9.793
$f_{A,1,6}$	-3.235	-0.470	$f_{B,1,6}$	1.745	9.490
$f_{A,1,7}$	-3.237	-0.474	$f_{B,1,7}$	1.749	9.497
$f_{A,1,8}$	-3.235	1.530	$f_{B,1,8}$	1.746	11.492

The concentration models proposed by the GP algorithm, optimized by the optimization routine and selected by the AIC are shown in Figure 4 below. Qualitatively, the proposed concentration models fit the data quite well. Although no physical constraints were imposed, it is important to mention that the chosen concentration profiles respect the law of conservation of mass (i.e.: $C_A + C_B = C_{A0} + C_{B0} = 2 + 0 = 2$ M, substituting the chosen models, $C_A + C_B = \exp k_1 - t + k_2 + k_3 - k_4 \exp -t = \exp k_1 \exp -t + k_2 + k_3 - k_4 \exp -t = k_1 \exp -t + k_2 + k_3 - k_4 \exp -t$, so if $k_1 = k_4$ and $k_2 + k_3 = 2$, then the law is respected) and their end-behavior are correct (i.e.: at time $t = 0$ s, $C_A \approx 2$ M and $C_B \approx 0$ M; at time $t \rightarrow \infty$, $C_A \approx 0.6$ M and $C_B \approx 1.4$ M). However, it should be noted that this observation is only valid for this case study; it is not certain that this behavior is displayed in other case studies. Notwithstanding, it is encouraging to see that ADoK-S, without enforcing constraints, recommends concentration profiles that respect the conservation of mass and the reached equilibrium of the system.

Following the ADoK-S flowchart presented in Figure 1, the next step is to compute the derivatives of the concentration profiles. In Figure 4, a plot of the numerical derivatives of concentration of A and B with respect to time is presented, along with the (realistically inaccessible) rate measurements.

Once the numerical derivative (i.e.: rate) data are estimated for each of the experiments, the GP algorithm is executed again, but this time to find a unifying rate equation that minimizes the error from its evaluation and the rate data. For this execution of the GP algorithm, it is specified that the proposed models should include the same operators as the concentration profile models, with the exception of the ‘exp’ operator. That is, the proposed rate models may include: ‘+’, ‘−’, ‘×’ and ‘/’. According to physical knowledge this is, once again, a fair selection of operators as the likelihood of these operators appearing in a rate model is very high. The flexibility of choosing different operators shows one way in which prior domain knowledge can be injected into kinetic model discovery (another way would be to constrain the algorithm, but this is outwith the scope of the investigation). Additionally, provided by prior knowledge, the proposed rate models may include concentrations of the observed species as variables: ‘ C_A ’ and ‘ C_B ’ in this case. The GP algorithm proposed the rate model structures shown below:

$$r_1 = k_1 \quad (15a)$$

$$r_2 = k_1 C_A \quad (15b)$$

$$r_3 = \frac{k_1 C_A}{k_2 C_B + k_3} \quad (15c)$$

$$r_4 = \frac{k_1 C_A - k_2 C_B}{k_3 C_A} \quad (15d)$$

$$r_5 = \frac{k_1 C_A - k_2 C_B + k_3}{k_4 C_A + k_5} \quad (15e)$$

$$r_6 = \frac{k_1 C_A - k_2 C_B - k_3}{k_4 C_A + k_5 C_B + k_6} \quad (15f)$$

$$r_7 = \frac{k_1 C_A^2 + k_2 C_A C_B - k_3 C_A - k_4 C_B^2}{k_5 C_A^2 + k_6 C_A C_B + k_7 C_A + k_8 C_B^2} \quad (15g)$$

where k_i for $i \in [1, 2, \dots, 8]$ are the parameters that are estimated according to the concentration data. To do so, the proposed rate models are integrated and evaluated at each time-step, given the initial conditions $C_{A,0}$ and $C_{B,0}$. Once again, the parameter estimation problem is solved by minimizing the NLL using the optimization routine comprised of the ABC and LBFGS algorithms. Table 2 clearly shows the NLL value along with the AIC values for each of the rate models, showing that r_6 is the best model for to represent the dynamical catalytic reactive system under investigation.

Table 2: The negative log likelihood values and the AIC values of all proposed rate models by ADoK-S.

Model	NLL Value	AIC Value
r_1	530.768	1063.535
r_2	61.304	124.608
r_3	5.187	16.373
r_4	1.301	8.601
r_5	-1.124	7.751
r_6	-2.419	7.161
r_7	-2.349	11.301

The response of the rate model proposed by the GP algorithm and selected by the AIC is shown in Figure 4. Qualitatively, once again, the proposed rate model fits the data extremely well, especially considering that only three computational experiments with 10 time-steps each were ran (i.e.: 60 datapoints).

Nevertheless, recalling the correct model structure presented in Equation 8, it is evident that the rate model selected has one extra parameter in the numerator. In fact, none of the rate equations proposed by SR retrieves the exact structure of the data-generating model. After performing parameter estimation on the selected model, the parameters obtained are presented in Table 3.

The first thing that can be perceived from Table 3 is that the extra parameter in the numerator of model r_6 is estimated to be zero. In other words, the GP algorithm was not able to retrieve the exact model structure, but the optimization routine determined that the extra parameter should be non-existent, arguably retrieving the correct model structure.

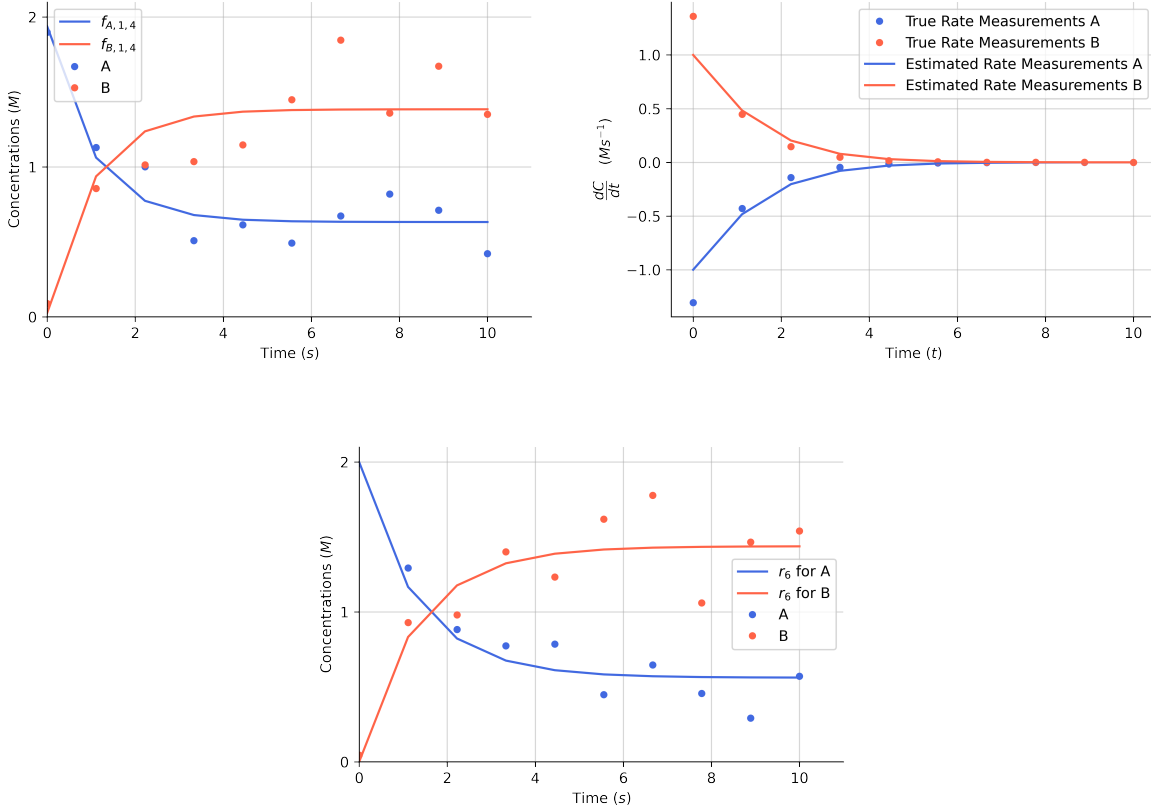


Figure 4: The conditions for the first computational experiment are $C_{A,0} = 2$ M and $C_{B,0} = 0$ M. Top left: Data from the first computational experiment and the selected concentration profiles selected by AIC. Top right: Numerical derivatives of the concentration profiles for and the true rate measurements (which realistically are inaccessible) for the first computational experiment. Bottom: Response of the selected GP-proposed rate model using ADoK-S for the first computational experiment.

Table 3: The data-generating kinetic parameters and the estimated values of the kinetic parameters of the ADoK-S selected model.

Kinetic Parameter	Estimated Value	True Value
k_1 / k_A	5.897 M s ⁻²	7.000 M s ⁻²
k_2 / k_B	2.302 M s ⁻²	3.000 M s ⁻²
k_3	0.000 M ² s ⁻²	N/a
k_4 / k_C	2.613 s ⁻¹	4.000 s ⁻¹
k_5 / k_D	3.182 s ⁻¹	2.000 s ⁻¹
k_6 / k_E	5.033 M s ⁻¹	6.000 M s ⁻¹

The second thing that can be perceived is that the estimated kinetic parameters are slightly different from the kinetic parameters that were used to generate the data. Of course, this is unsurprising due to the additive Gaussian noise that was introduced in the dataset. Had the parameter uncertainty been calculated, chances are that the true parameters would lie within the 95% confidence interval, given the small difference between the true and the estimated values (notwithstanding, this is pure conjecture as parameter uncertainty was outside the scope of this investigation).

To briefly summarize, the results demonstrated that ADoK-S is robust to noise, regardless of the fact that derivatives needed to be calculated numerically. The main reason for the robustness of the method stems from utilizing GP and AIC to generate and select, respectively, good concentration models that do not overfit the data. In this way, the numerical derivatives continue to have a high degree of accuracy. The final rate model output by ADoK-S had a near identical

structure to the data-generating one, differing only by a single parameter in the numerator. However, after performing parameter estimation, the extra parameter was determined to be practically zero, and therefore should not appear in the proposed model. The other estimated kinetic parameters, although not identical to the true values, they were close to them. All in all, ADoK-S is capable of retrieving the underlying kinetic rate model of a catalytic isomerization reaction with realistic data.

4.2 Isomerization Reaction — ADoK-W

As explained in Section 2.2, ADoK-W aims to solve a weak formulation of symbolic regression by implementing GP. In this methodological framework, departing from the kinetic data generated, the GP algorithm instead of generating concentration profile models and then kinetic rate models, it automatically evolves rate models by integrating and comparing them with the concentration data available directly. Note that the law of conservation of mass is satisfied by construction under this integrating scheme. The expression construction rules exclusively included the arithmetic operators '+', '-', '×' and '/', since rates including other operators are less common. Alike in ADoK-S, the kinetic rate models generated are allowed to be a function of the species whose concentrations were measured, $r(C_A, C_B)$ in this case. The best expression proposed by the GP algorithm, sorted by degree of complexity (i.e.: the number of operators and variables), are shown below.

$$r_1 = k_1 \tag{16a}$$

$$r_2 = k_1 C_A \tag{16b}$$

$$r_3 = \frac{k_1 C_A - k_2 C_B}{k_3 C_A} \tag{16c}$$

$$r_4 = \frac{k_1 C_A - k_2 C_B - k_3}{k_4 C_A} \tag{16d}$$

$$r_5 = \frac{k_1 C_A - k_2 C_B - k_3}{k_4 C_A + k_5} \tag{16e}$$

$$r_6 = \frac{k_1 C_A - k_2 C_B - k_3}{k_4 C_A + k_5 C_B + k_6} \tag{16f}$$

$$r_7 = \frac{k_1 C_A^2 C_B - k_2 C_A C_B^2 - k_3 C_A + k_4 C_B}{k_5 C_A^2 C_B - k_6 C_A} \tag{16g}$$

The estimation of each kinetic parameter, k_i for $i \in [1, 2, \dots, 6]$, is carried out as explained previously: NLL is used as the objective function where the assumed variances are double of the real variances used to generate the additive Gaussian noise, and this is solved by deploying the optimization routine consisting of the ABC and the LBFGS algorithms. Table 4 clearly shows the NLL value along with the AIC values for each of the rate models, showing that r_6 is the best model for the given dataset.

Table 4: The negative log likelihood values and the AIC values of all proposed rate models by ADoK-W.

Model	NLL Value	AIC Value
r_1	540.410	1082.821
r_2	53.857	109.715
r_3	-0.831	4.337
r_4	-0.988	6.025
r_5	-2.724	4.551
r_6	-4.275	3.450
r_7	-2.289	7.422

The response of the selected model is shown in Figure 5. For the sake of brevity, only one of the experiments is presented. The final rate model output by the proposed framework had a near identical structure to the data-generating one, differing only by a single parameter in the numerator, displaying an identical result to ADoK-S. And once again, the optimization routine used to solve the parameter estimation problem is able to determine that the extra parameter is practically zero, and therefore may be non-existent in the actual model. In this case, since the data-generating model is known, we can indeed validate this conclusion which would have naturally been made regardless of having access to

the underlying ground-truth model or not.

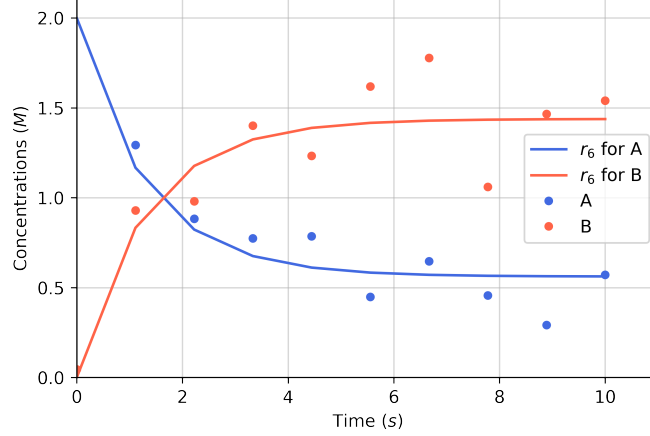


Figure 5: Response of the selected GP-proposed rate model using ADoK-W for the first computational experiment where $C_{A,0} = 2$ M and $C_{B,0} = 0$ M.

Similar to the estimated kinetic parameter values presented in Table 3, Table 5 also shows that the estimated kinetic parameters are slightly different from the true values. As previously explained, this discrepancy is caused by the additive Gaussian noise. It should be noted that the value of NLL for r_6 in Table 2 and in Table 4 (r_6 is identical for both approaches) are slightly different. The reason being that the estimated parameters are different for both approaches. This finding can be attributed to the optimization algorithm not finding the global optimum and getting stuck in different local optima in different runs.

Table 5: The data-generating kinetic parameters and the estimated values of the kinetic parameters of the ADoK-W selected model.

Kinetic Parameter	Estimated Value	True Value
k_1 / k_A	5.557 M s^{-2}	7.000 M s^{-2}
k_2 / k_B	2.335 M s^{-2}	3.000 M s^{-2}
k_3	$0.000 \text{ M}^2 \text{ s}^{-2}$	N/a
k_4 / k_C	3.114 s^{-1}	4.000 s^{-1}
k_5 / k_D	1.379 s^{-1}	2.000 s^{-1}
k_6 / k_E	6.033 M s^{-1}	6.000 M s^{-1}

One thing that should be mentioned about ADoK-W is the computational time. On one hand, the GP-steps of ADoK-S (i.e.: proposing concentration profiles and rate models) takes in the order of minutes to be completed. For this particular case study, it took around 10 minutes to propose 6 concentration models (2 concentration profiles, one for A and one for B, for each of the three experiments) and 1 rate model using an Apple MacBook Air (M1, 2020). On the other hand, the GP-step in ADoK-W (i.e.: proposing rate models) take in the order of hours to be completed. For this particular case study, it took around 5 hours to propose 1 rate model using the high performance computing cluster with 8-core CPU configured with 64GB of RAM. This is unsurprising, as in ADoK-W, to calculate the fitness value of each of the proposed rate models, numerical integration needs to be performed. For ADoK-S, the fitness values are calculated by merely evaluating a function. Therefore, ADoK-W builds resilience to noise by making it more computationally intensive. This could have ramifications as to the amount of data that this approach could take before it becomes intractable.

The results demonstrated that ADoK-W, as expected from a weak formulation, is robust to noise. The final rate model output by ADoK-W has a near identical structure to the data-generating one, differing only by a single parameter in the numerator. However, the optimization algorithm used for parameter estimation is able to determine that the

extra parameter was practically zero, and therefore should be removed from the model. The other estimated kinetic parameters are, although not identical to the true values, close to them. In this way, ADoK-W and ADoK-S were identical. However, in computational time, they were noticeably different, where ADoK-S took in the order of minutes to terminate and ADoK-W took in the order of hours. It has been hypothesized that ADoK-W might be successful in highly noisy environments where ADoK-S might fail, but it might also be intractable in the high-data regime where ADoK-S might still be tractable. All in all, ADoK-W, alike ADoK-S, is capable of retrieving the underlying kinetic rate model of a catalytic isomerization reaction with realistic data.

4.3 Decomposition of Nitrous Oxide — ADoK-S

As shown in Figure 1, the first step of ADoK-S is to generate concentration profiles, perform parameter estimation on the the proposed models, and with AIC select the best model. For the catalytic decomposition of nitrous oxide, ADoK-S selected the following concentration profiles for each species in each experiment.

$$f_{N_2O,1} = \exp(1.587 - 0.357t) \quad (17a)$$

$$f_{N_2,1} = t - \exp(0.192t) + 1.683 \quad (17b)$$

$$f_{O_2,1} = 0.395 \exp(2.320179 - t) + 3.630 \quad (17c)$$

$$f_{N_2O,2} = \exp(2.023 - 0.386t) \quad (17d)$$

$$f_{N_2,2} = \exp \left[\exp \left(\frac{t}{\frac{t}{0.908} + 1.147} \right) \right] - 1.198 \quad (17e)$$

$$f_{O_2,2} = \frac{5.516}{\exp(\exp(-0.586t))} \quad (17f)$$

$$f_{N_2O,3} = \exp(2.023 - 0.386t) \quad (17g)$$

$$f_{N_2,3} = 3.081t + 1.540 - (0.240 - 0.010t)(t - \exp(1.643 - 2t)) \quad (17h)$$

$$f_{O_2,3} = \exp(2.058 - \exp(-0.597t)) \quad (17i)$$

For the sake of brevity, the concentration models proposed by the GP algorithm, optimized by the optimization routine and selected by the AIC are shown only for the second experiment in Figure 6 below. The selected concentration profiles, qualitatively, fit the concentration data well.

Once established the selected concentration models, the rate measurements (i.e.: derivatives of the concentration profiles) are estimated. Below, a plot of the numerical derivatives and (realistically inaccessible) rate measurements is presented. From this plot, we can conclude that the rate measurements are indeed accurately estimated.

After estimating the rate measurements of the catalytic system, rate models are proposed using the GP algorithm and optimized. The best model is then selected by AIC, which for this case study, it is shown below.

$$r = \frac{C_{N_2O}^2}{k'_1 + k'_2 C_{N_2O}} = \frac{k_1 C_{N_2O}^2}{1 + k_2 C_{N_2O}} \quad (18)$$

The response of the selected model is shown in Figure 6. Qualitatively, once again, the proposed rate model fits the data extremely well, especially considering that only three computational experiments with 10 time-steps each were ran (i.e.: 90 datapoints). Furthermore, recalling the correct model structure presented in Equation 10, with some simple algebraic manipulation (multiplying numerator and denominator by $\frac{1}{k'_1}$), the same form is retrieved, as shown in Equation 18.

Table 6 shows the comparison between the kinetic parameters used to generate the data of the homogeneous decomposition of nitrous oxide and the estimated values of these parameters. Alike the previous case study, the estimated kinetic parameters are slightly different from the true ones, which is unsurprising given the additive Gaussian noise. All in all, ADoK-S is capable of retrieving the underlying kinetic rate model of the catalytic decomposition of nitrous oxide with realistic data.

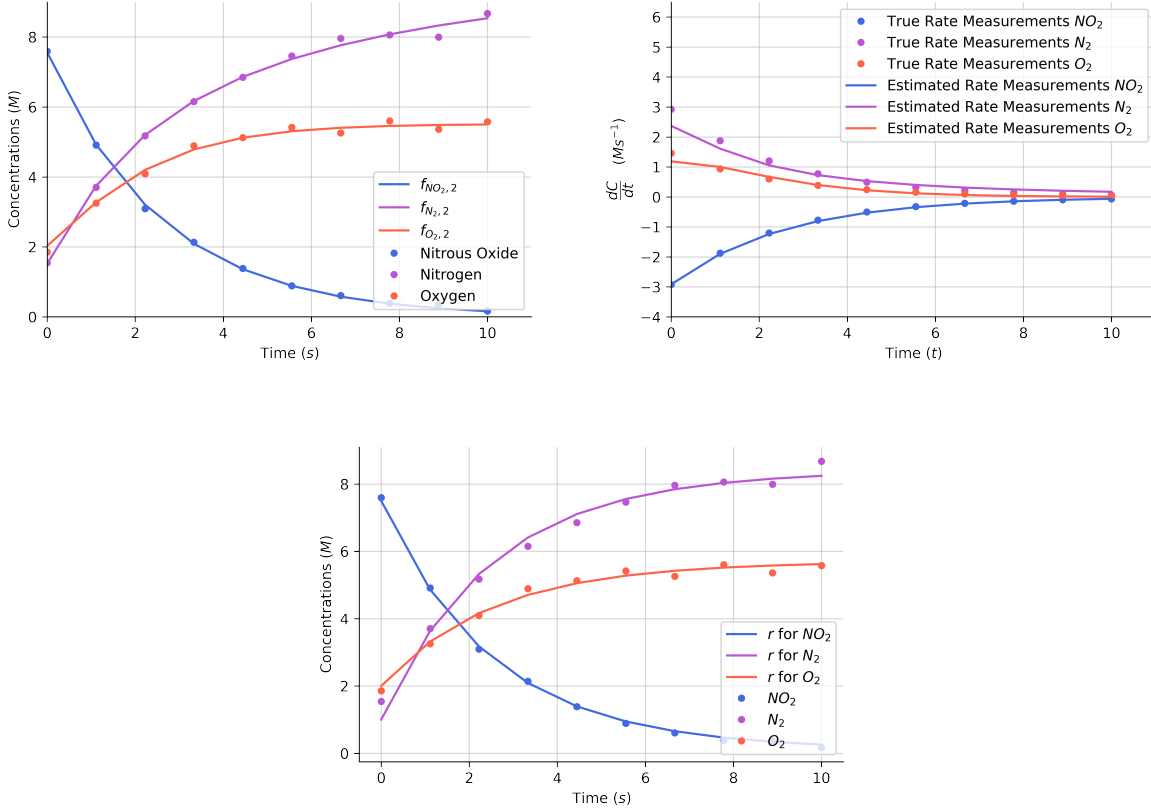


Figure 6: The conditions for the second computational experiment are $C_{N_2O,0} = 7.5\text{M}$, $C_{N_2,0} = 1\text{M}$ and $C_{O_2,0} = 2\text{M}$. Top left: Data from the second computational experiment and the selected concentration profiles selected by AIC. Top right: Numerical derivatives of the concentration profiles and the true rate measurements (which realistically are inaccessible) for the second computational experiment. Bottom: Response of the selected GP-proposed rate model using ADoK-S for the second computational experiment.

Table 6: The data-generating kinetic parameters and the estimated values of the kinetic parameters of the ADoK-S selected model for the catalytic decomposition of nitrous oxide.

Kinetic Parameter	Estimated Value	True Value
k_1 / k_A	$2.332 \text{ M}^{-1} \text{ s}^{-1}$	$2.000 \text{ M}^{-1} \text{ s}^{-1}$
k_2 / k_B	5.811 M^{-1}	5.000 M^{-1}

4.4 Decomposition of Nitrous Oxide — ADoK-W

As shown in Figure 2, ADoK-W combines the two steps of the other proposed methodology into a single one by solving the symbolic regression problem in his weak formulation. The selected model by the approach is:

The response of the selected model is shown in Figure 7. Identically to the results presented in the previous section, recalling the correct model structure presented in Equation 10, with some simple algebraic manipulation (multiplying numerator and denominator by $\frac{1}{k_1}$), the same form is retrieved, as shown in Equation 18.

Table 7 shows the comparison between the kinetic parameters used to simulate the homogeneous decomposition of nitrous oxide and the estimated values of these parameters. Alike the previous case study, the estimated kinetic parameters are slightly different from the true ones, which is unsurprising given the additive Gaussian noise. All in all, the ADoK-W is capable of retrieving the underlying kinetic rate model of the catalytic decomposition of nitrous oxide

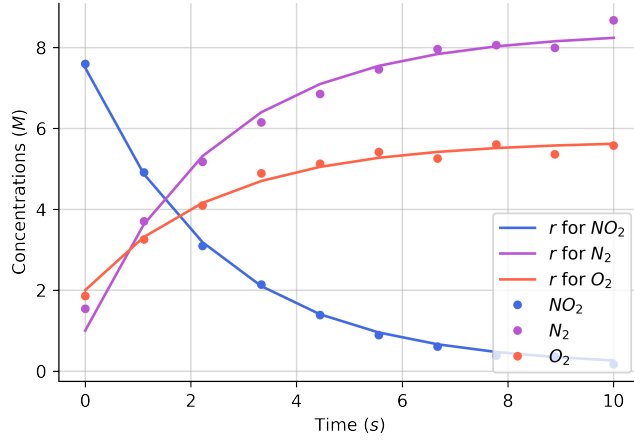


Figure 7: Response of the selected GP-proposed rate model using ADoK-W for the second computational experiment where $C_{N_2O,0} = 7.5$ M, $C_{N_2,0} = 1$ M and $C_{O_2,0} = 2$ M.

with realistic data.

Table 7: The data-generating kinetic parameters and the estimated values of the kinetic parameters of the ADoK-W selected model for the catalytic decomposition of nitrous oxide.

Kinetic Parameter	Estimated Value	True Value
k_1 / k_A	$2.322 \text{ M}^{-1} \text{ s}^{-1}$	$2.000 \text{ M}^{-1} \text{ s}^{-1}$
k_2 / k_B	5.811 M^{-1}	5.000 M^{-1}

4.5 Toluene Hydrodealkylation — ADoK-S

For the catalytic hydrodealkylation of toluene to benzene, ADoK-S selected the following concentration profiles for each species in each experiment.

$$f_{T,1} = \frac{1.115}{0.316t^2 + t + 1.074} \quad (19a)$$

$$f_{H,1} = \exp(-0.510t) + 1.975 \quad (19b)$$

$$f_{B,1} = \exp\left(\frac{-3.160}{t + \exp(t)}\right) \quad (19c)$$

$$f_{M,1} = \frac{-0.719}{\exp(t)} + 1.407 \quad (19d)$$

$$f_{T,2} = \exp(t + 0.195 \exp(0.568 - t) + 0.781) \quad (19e)$$

$$f_{H,2} = \exp\left[\exp\left(\frac{1.132 - t}{4.222}\right) + 1.794\right] \quad (19f)$$

$$f_{B,2} = \frac{t}{\frac{t}{3.658} + 0.900} + 1.012 \quad (20a)$$

$$f_{M,2} = \frac{t - 4.885}{t + 1.971} + 3.985 \quad (20b)$$

$$f_{T,3} = \exp(\exp(-0.099(2t - 4.791))) - 0.042t \quad (20c)$$

$$f_{H,3} = \exp(\exp(-0.218(t + 0.971)) + 1.267) \quad (20d)$$

$$f_{B,3} = \frac{t}{\exp(\frac{t}{10.001})} + 2.361 \quad (20e)$$

$$f_{M,3} = \frac{-16.919}{t + 2.985} + 8.488 \quad (20f)$$

In the expressions above, T , H , B and M refer to toluene, hydrogen, benzene and methane, respectively. For the sake of brevity, the concentration models proposed by the GP algorithm, optimized by the optimization routine and selected by the AIC are only shown for the third experiment in Figure 8 below. The selected concentration profiles, qualitatively, fit the concentration data well.

As shown in Figure 1, once the concentration profiles are modeled, the parameters estimated, and the best model selected, the rate measurements (i.e.: derivatives of the concentration profiles) are approximated. Below, a plot of the

numerical derivatives and (realistically inaccessible) rate measurements is presented. From this plot, we can conclude that the rate measurements are fairly well estimated. However, significant discrepancies can be appreciated at the start of the graph for the rate of production of benzene, showing that the initial curvature of the concentration profile for benzene is not well captured.

After estimating the rate measurements of the catalytic system, rate models are proposed using the GP algorithm and optimized. The best model is then selected by AIC, which for this case study, it is shown below.

$$r = \frac{k_1 C_T C_H}{k_2 + k_3 C_B + k_4 C_H} \quad (21)$$

Recalling the correct model structure presented in Equation 12, the proposed kinetic rate model from ADoK-S is not identical to it. Although the proposed model is very similar to the correct one, it differs only in one variable in the denominator (C_H should be C_T). This result is unsurprising, since the profile of hydrogen and toluene are nearly identical, simply differing by a constant scaling factor (as both species have the same stoichiometric coefficients but different initial concentrations). As such, knowing the data-generating model a priori, as modelers, we are not satisfied and should then perform additional experiments. For the purpose of this investigation, we limit the experimental budget to 4 experiments.

To demonstrate the potential of the case study, model-based design of experiments is conducted. Specifically, the Hunter-Reiner criterion is used, where an experimental point is found which maximizes the difference between two models' responses Hunter and Reiner [1965]. Alike the parameter estimation, the optimization routine outlined which harnesses the output of the ABC algorithm to warm-start the LBFGS algorithm is used to solve the Hunter-Reiner criterion, where the two models under question are Equation 12 (ground-truth model) and Equation 21 (ADoK-S proposed model). The optimized experimental point is $(C_{T,0}, C_{H,0}, C_{B,0}, C_{M,0}) = (5, 3, 0, 2.276)$. Realistically, this exercise could not be undertaken, since the underlying dynamic model would not be available. Regardless, as mentioned before, this exercise is meant to investigate the potential of the methodological framework proposed. One thing should be mentioned however: the initial experiments conducted are randomly selected, which is not an optimal methodology. In practice, statistic design of experiments should be initially used to carefully select experiments, so that the generated dynamic trajectories are sufficiently different, the process information gain can be maximized and the experimental expense can be minimized. This would improve the effectiveness of the proposed methodologies.

As per the flowchart presented in Figure 1, after generating new experiments, the algorithm must be repeated for the appended computational experiment. The resulted new best rate model selected by AIC is shown below.

$$r = \frac{k'_1 C_T C_H}{k'_2 C_B + C_T + k'_3} = \frac{k_1 C_T C_H}{1 + k_2 C_B + k_3 C_T} \quad (22)$$

By undergoing simple algebraic manipulation (multiplying the numerator and denominator by a factor of $\frac{1}{k'_3}$), the proposed model (Equation 22) is identical to the data-generating kinetic rate model (Equation 12). The response of the selected kinetic rate model is shown below in Figure 8, whilst the estimation of the corresponding kinetic parameters are presented in Table 8.

Table 8: The data-generating kinetic parameters and the estimated values of the kinetic parameters of the ADoK-S selected model for the catalytic hydrodealkylation of toluene to benzene.

Kinetic Parameter	Estimated Value	True Value
k_1 / k_A	$1.922 \text{ M}^{-1} \text{ s}^{-1}$	$2.000 \text{ M}^{-1} \text{ s}^{-1}$
k_2 / k_B	8.726 M^{-1}	9.000 M^{-1}
k_3 / k_C	4.656 M^{-1}	5.000 M^{-1}

From these results we can conclude that, although ADoK-S is not able to return the correct kinetic rate model from a small dataset composed of three random experiments, it is still able to return a model very similar to the ground-truth one. Notwithstanding, provided more data from a single extra experiment, ADoK-S is able to select an identical kinetic rate model whilst estimating the corresponding kinetic parameters reasonably well.

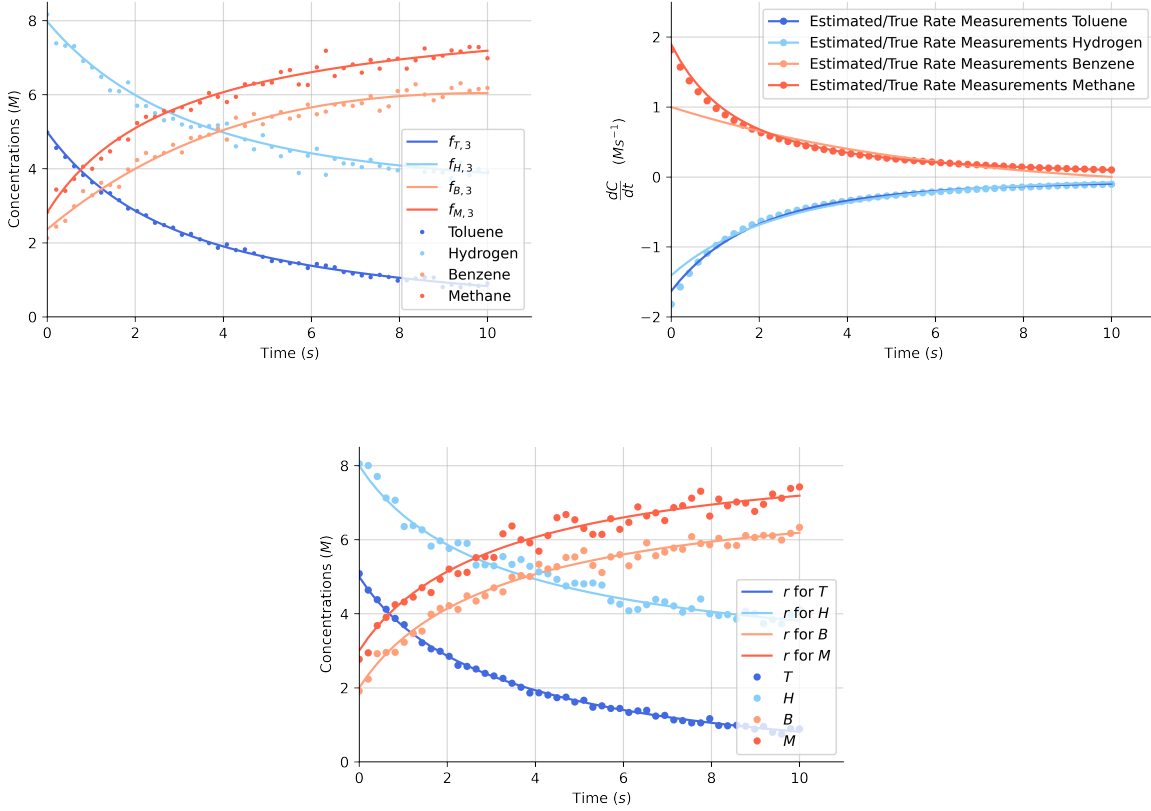


Figure 8: The conditions for the third computational experiment are $C_{T,0} = 5$ M, $C_{H,0} = 8$ M, $C_{B,0} = 2$ M and $C_{M,0} = 3$ M. Top left: Data from the third computational experiment and the selected concentration profiles selected by AIC. Top right: Numerical derivatives of the concentration profiles and the true rate measurements (which realistically are inaccessible) for the third computational experiment. Bottom: Response of the selected GP-proposed rate model using ADoK-S for the third computational experiment.

4.6 Toluene Hydrodealkylation — ADoK-W

Similarly to the behavior of ADoK-S on the catalytic hydrodealkylation of toluene to benzene, the 1-step approach is unable to produce the true underlying kinetic model from the three initial computational experiments. The initially selected model is presented below.

$$r = \frac{k_1(C_H + k_2)(C_T - k_3)}{C_B + C_T} \quad (23)$$

Recalling the correct model structure presented in Equation 12, the proposed kinetic rate model from ADoK-W is quite different from it. As such, like in the previous example, we are not satisfied with the model and should then perform additional experiments. For the purpose of this investigation, we limit the experimental budget to 4 experiments.

Model-based design of experiments is conducted yet again using the Hunter-Reiner criterion and the optimization routine to solve it. The optimized experimental point is $(C_{T,0}, C_{H,0}, C_{B,0}, C_{M,0}) = (5, 7.302, 0, 2.247)$. Realistically, this exercise could not be undertaken, since the underlying dynamic model would not be available. Regardless, as mentioned, this exercise is meant to investigate the potential of the methodological framework proposed.

As per the flowchart presented in Figure 2, after generating new experiments, the algorithm must be repeated for the appended computational experiment, just like for ADoK-S. The new best rate model selected by AIC is shown below. As demonstrated, with one additional computational experiment, ADoK-W is also able to retrieve the dynamics of

the catalytic system. This allows us to conclude that as the complexity of a system under investigation increases, the required amount of data provided to both approaches must increase accordingly. In this context, ‘complexity’ refers not only to the number of species that can be directly observed, but also to the level of convolution of the underlying dynamics. For completeness, Figure 9 presents the behavior of the model selected by ADoK-W, along with Table 9 which presents the estimated values (and the true values) of the kinetic parameters.

$$r = \frac{k'_1 C_T C_H}{k'_2 C_B + C_T + k'_3} = \frac{k_1 C_T C_H}{1 + k_2 C_B + k_3 C_T} \quad (24)$$

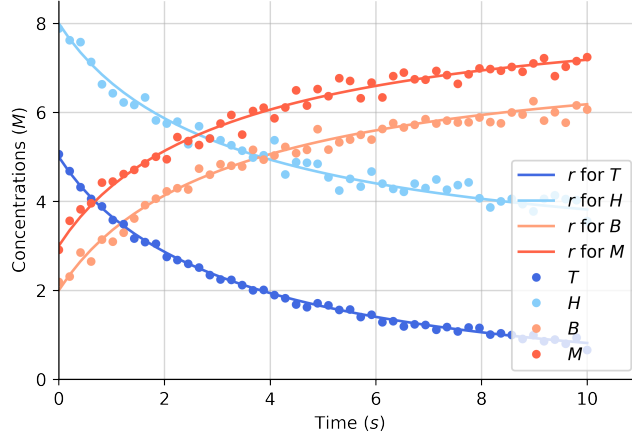


Figure 9: Response of the selected GP-proposed rate model using ADoK-W for the second computational experiment where $C_{T,0} = 5$ M, $C_{H,0} = 8$ M, $C_{B,0} = 2$ M and $C_{M,0} = 3$ M.

Table 9: The data-generating kinetic parameters and the estimated values of the kinetic parameters of the ADoK-W selected model for the catalytic hydrodealkylation of toluene to benzene.

Kinetic Parameter	Estimated Value	True Value
k_1 / k_A	$2.190 \text{ M}^{-1} \text{ s}^{-1}$	$2.000 \text{ M}^{-1} \text{ s}^{-1}$
k_2 / k_B	10.000 M^{-1}	9.000 M^{-1}
k_3 / k_C	5.340 M^{-1}	5.000 M^{-1}

5 Conclusions

Kinetic rate models are indispensable for the successful development of catalytic processes. Classical modeling paradigms offer strategies to construct these models, some of which are well established in industry, others which are becoming more prevalent. Regardless, these classical paradigms demonstrate some noteworthy challenges: the construction of mechanistic models are expensive and time-consuming, whilst data-driven and hybrid models are mostly uninterpretable and usually lack the ability to extrapolate. Automated knowledge discovery, a newer paradigm, aims to harness machine learning and computational advances to generate closed-form models and circumvent these challenges. Nevertheless, popularized methodologies within automated knowledge discovery also demonstrate notable drawbacks: usually requiring limiting assumptions about an underlying model structure, a general lack of a robust and motivated model selection routine, and sensitivity to noisy data.

These limitations motivated the presented work to explore and propose two different methodological frameworks for the automated discovery of kinetic rate models. The first one, ADoK-S, explores how to solve a strong formulation of the symbolic regression problem. It does so by exploiting a genetic programming algorithm to automatically generate closed-form concentration profile models, a sequential optimization routine to refine the most promising generated kinetic models, and the Akaike information criterion to selected the best model (it is important to mention that this criterion has been selected due to a thorough analysis conducted on different model selection criteria which concluded

that AIC is the most robust one). Once the best concentration model is selected, rate measurements are estimated via numerical differentiation, and the mentioned routine of model generation, model refinement and model selection is repeated to discover kinetic rate models.

As referred, ADoK-S needs to estimate rate measurements through numerical differentiation, which can be problematic under high-noise environments. To guard against this potential downside of ADoK-S, another methodological framework was proposed, ADoK-W, which explores how to solve a weak formulation of the symbolic regression problem. By reformulation the problem to its weak form, the step to propose concentration models and estimate rate measurements is bypassed. Instead, kinetic rate models can be proposed from the start by working in the derivative hyperspace. In ADoK-W, alike ADoK-S, models are generated with a genetic programming algorithm, the most promising models are refined using a sequential optimization routine, and the best kinetic rate model is selected by AIC.

To benchmark both approaches, three catalytic case studies (of increasing complexity) were carefully selected: a simple isomerization reaction, the decomposition of nitrous oxide, and the hydrodealkylation of toluene. Both approaches successfully retrieved the underlying dynamics of the isomerization reaction and of the decomposition of nitrous oxide with three pseudo-randomized computational experiments. However, neither approach was able to retrieve the ground-truth kinetic model for the hydrodealkylation of toluene case study. Nonetheless, to prove the potential of the methodological frameworks, an extra experiment was appended to the original dataset. This experiment was determined by solving the Hunter-Reiner criterion between the data-generating model and the methodology-selected model. By adding one extra experiment, both approaches successfully recovered the kinetics, concluding that as the complexity of the system increases, so must the data (information) provided to ADoK-S and ADoK-W. As previously referred, the methodologies could be more efficient by implementing statistic design of experiments in the first step of the frameworks, so that the experiments generated are optimal rather than random.

As such, it is fair to conclude that the proposed methodologies build-on from previously presented approaches to automated knowledge discovery by tackling identified shortcomings directly. From this investigations, new angles of research arose which will be investigated in future work. For instance: the frameworks should be stress-tested with respect to noise and quantity of data; the introduction of physical and mathematical constraints should be explored and assessed with respect to the efficacy of ADoK-S and ADoK-W; investigate possible ways to approximate optimal experiments without having direct access to the underlying dynamics model; lastly, research how the methodological frameworks can be harnessed to uncover how temperature (and other variables, such as the morphology of a catalyst) affect the rate of a reaction. But for now, with the provided study, we believe that these methodologies can be successfully applied to aid chemical reaction engineers in solving current and future problems.

References

- R. E. Baker, J. M. Peña, J. Jayamohan, and A. Jérusalem. Mechanistic models versus machine learning, a fight worth fighting for the biological community? *Biol. Lett.*, 14(5):20170660, May 2018. doi:10.1098/rsbl.2017.0660.
- G.C. Battiston, L. Dalloro, and G.R. Tauszik. Performance and aging of catalysts for the selective hydrogenation of acetylene: a micropilot-plant study. *Appl. Catal.*, 2(1-2):1–17, January 1982. doi:10.1016/0166-9834(82)80170-x.
- D. Bertsimas and W. Gurnee. Learning Sparse Nonlinear Dynamics via Mixed-Integer Optimization. *arXiv:2206.00176*, 2022. doi:10.48550/ARXIV.2206.00176.
- D. Brockmann, L. Hufnagel, and T. Geisel. The scaling laws of human travel. *Nature*, 439(7075):462–465, January 2006. doi:10.1038/nature04292.
- S. L. Brunton, J. L. Proctor, and J. N. Kutz. Discovering governing equations from data by sparse identification of nonlinear dynamical systems. *Proc. Natl. Acad. Sci. U.S.A.*, 113(15):3932–3937, March 2016. doi:10.1073/pnas.1517384113.
- B. A. Cho, M. Á. de Carvalho Servia, E. A. del Rio Chanona, R. Smith, and D. Zhang. Synergising biomass growth kinetics and transport mechanisms to simulate light/dark cycle effects on photo-production systems. *Biotechnol. Bioeng.*, 118(5):1932–1942, March 2021. doi:10.1002/bit.27707.
- M. Cranmer. PySR: Fast & Parallelized Symbolic Regression in Python/Julia, September 2020.
- E. A. del Rio-Chanona, X. Cong, E. Bradford, D. Zhang, and K. Jing. Review of advanced physical and data-driven models for dynamic bioprocess simulation: Case study of algae–bacteria consortium wastewater treatment. *Biotechnol. Bioeng.*, 116(2):342–353, December 2018a. doi:10.1002/bit.26881.

- E. A. del Rio-Chanona, J. L. Wagner, H. Ali, F. Fiorelli, D. Zhang, and K. Hellgardt. Deep learning-based surrogate modeling and optimization for microalgal biofuel production and photobioreactor design. *AIChE J*, 65(3):915–923, December 2018b. doi:10.1002/aic.16473.
- H. S. Fogler. *Elements of chemical reaction engineering*. Prentice Hall, Philadelphia, PA, 5 edition, January 2016.
- L. C. Franssen, T. Lorenzi, A. E. F. Burgess, and M. A. J. Chaplain. A Mathematical Framework for Modelling the Metastatic Spread of Cancer. *Bull. Math. Biol.*, 81(6):1965–2010, March 2019. doi:10.1007/s11538-019-00597-x.
- K. V. Gernaey. A Perspective on PSE in Fermentation Process Development and Operation. *Comput. Aided Chem. Eng.*, pages 123–130, 2015. doi:10.1016/b978-0-444-63578-5.50016-5.
- C. Haider, F.O. de Franca, B. Burlacu, and G. Kronberger. Shape-constrained multi-objective genetic programming for symbolic regression. *Appl. Soft Comput.*, 132:109855, January 2023. doi:10.1016/j.asoc.2022.109855.
- A. C. Hindmarsh and L. R. Petzold. LSODA, Ordinary Differential Equation Solver for Stiff or Non-Stiff System, September 2005.
- J. D. Hunter. Matplotlib: A 2D graphics environment. *Comput Sci Eng*, 9(3):90–95, 2007. doi:10.1109/MCSE.2007.55.
- William G. Hunter and Albey M. Reiner. Designs for Discriminating Between Two Rival Models. *Technometrics*, 7(3): 307–323, August 1965. doi:10.1080/00401706.1965.10490265.
- P. Kadlec, B. Gabrys, and S. Strandt. Data-driven Soft Sensors in the process industry. *Comput Chem Eng.*, 33(4): 795–814, April 2009. doi:10.1016/j.compchemeng.2008.12.012.
- S. Kay, H. Kay, M. Mowbray, A. Lane, C. Mendoza, P. Martin, and D. Zhang. Integrating Autoencoder and Heteroscedastic Noise Neural Networks for the Batch Process Soft-Sensor Design. *Ind. Eng. Chem. Res.*, 61(36): 13559–13569, September 2022. doi:10.1021/acs.iecr.2c01789.
- J. R. Koza. Genetic programming as a means for programming computers by natural selection. *Stat Comput*, 4(2), June 1994. doi:10.1007/bf00175355.
- O. Levenspiel. *Chemical Reaction Engineering*. John Wiley & Sons, Nashville, TN, 3 edition, August 1998.
- D. C. Liu and J. Nocedal. On the limited memory BFGS method for large scale optimization. *Math. Program.*, 45(1-3): 503–528, August 1989. doi:10.1007/bf01589116.
- R. Malouf. A Comparison of Algorithms for Maximum Entropy Parameter Estimation. In *Proceedings of the 6th Conference on Natural Language Learning - Volume 20*, COLING-02, page 1–7, USA, 2002. Association for Computational Linguistics. doi:10.3115/1118853.1118871. URL <https://doi.org/10.3115/1118853.1118871>.
- D. H. Margarit and L. Romanelli. A mathematical model of absorbing Markov chains to understand the routes of metastasis. *Biomath*, 5(1), August 2016. doi:10.11145/j.biomath.2016.07.281.
- G. B. Marin, G. S Yablonsky, and D. Constales. *Kinetics of chemical reactions: decoding complexity*. John Wiley & Sons, 2019.
- M. Mowbray, H. Kay, S. Kay, P. Castro Caetano, A. Hicks, C. Mendoza, A. Lane, P. Martin, and D. Zhang. Probabilistic machine learning based soft-sensors for product quality prediction in batch processes. *Chemometr Intell Lab Syst*, 228:104616, September 2022a. doi:10.1016/j.chemolab.2022.104616.
- M. R. Mowbray, C. Wu, A. W. Rogers, E. A. del Rio-Chanona, and D. Zhang. A reinforcement learning-based hybrid modeling framework for bioprocess kinetics identification. *Biotechnol. Bioeng.*, 120(1):154–168, October 2022b. doi:10.1002/bit.28262.
- P. Natarajan, R. Moghadam, and S. Jagannathan. Online deep neural network-based feedback control of a Lutein bioprocess. *J. Process Control*, 98:41–51, February 2021. doi:10.1016/j.jprocont.2020.11.011.
- P. Neumann, L. Cao, D. Russo, V. S. Vassiliadis, and A. A. Lapkin. A new formulation for symbolic regression to identify physico-chemical laws from experimental data. *J. Chem. Eng.*, 387:123412, May 2020. doi:10.1016/j.cej.2019.123412.
- S. Y. Park, C. H. Park, D. H. Choi, J. K. Hong, and D. Y. Lee. Bioprocess digital twins of mammalian cell culture for advanced biomanufacturing. *Curr. Opin. Chem. Eng.*, 33:100702, September 2021. doi:10.1016/j.coche.2021.100702.
- P. Petsagkourakis, I. O. Sandoval, E. Bradford, D. Zhang, and E.A. del Rio-Chanona. Reinforcement learning for batch bioprocess optimization. *Comput Chem Eng.*, 133:106649, February 2020. doi:10.1016/j.compchemeng.2019.106649.
- N. S. Schbib, M. A. García, C. E. Gígola, and A. F. Errazu. Kinetics of Front-End Acetylene Hydrogenation in Ethylene Production. *Ind. Eng. Chem. Res.*, 35(5):1496–1505, January 1996. doi:10.1021/ie950600k.

- L. Schrecker, J. Dickhaut, C. Holtze, P. Staehle, M. Vranceanu, K. Hellgardt, and K. K. Hii. Discovery of unexpectedly complex reaction pathways for the Knorr pyrazole synthesis via transient flow. *React. Chem. Eng.*, 8(1):41–46, 2023. doi:10.1039/d2re00271j.
- C. Song, T. Koren, P. Wang, and A. L. Barabási. Modelling the scaling properties of human mobility. *Nat. Phys.*, 6(10): 818–823, September 2010. doi:10.1038/nphys1760.
- Y. Sun, W. Nathan-Roberts, T. D. Pham, E. Otte, and U. Aickelin. Multi-fidelity Gaussian Process for Biomanufacturing Process Modeling with Small Data. *arXiv:2211.14493*, 2022. doi:10.48550/ARXIV.2211.14493.
- C. J. Taylor, M. Booth, J. A. Manson, M. J. Willis, G. Clemens, B. A. Taylor, T. W. Chamberlain, and R. A. Bourne. Rapid, automated determination of reaction models and kinetic parameters. *J. Chem. Eng.*, 413:127017, June 2021. doi:10.1016/j.cej.2020.127017.
- F. Vega-Ramon, X. Zhu, T. R. Savage, P. Petsagkourakis, K. Jing, and D. Zhang. Kinetic and hybrid modeling for yeast astaxanthin production under uncertainty. *Biotechnol. Bioeng.*, 118(12):4854–4866, October 2021. doi:10.1002/bit.27950.
- P. Virtanen, R. Gommers, T. E. Oliphant, M. Haberland, T. Reddy, D. Cournapeau, E. Burovski, P. Peterson, W. Weckesser, J. Bright, S. J. van der Walt, M. Brett, J. Wilson, K. J. Millman, N. Mayorov, A. R. J. Nelson, E. Jones, R. Kern, E. Larson, C. J. Carey, Í. Polat, Y. Feng, E. W. Moore, J. VanderPlas, D. Laxalde, J. Perktold, R. Cimrman, I. Henriksen, E. A. Quintero, C. R. Harris, A. M. Archibald, A. H. Ribeiro, F. Pedregosa, P. van Mulbregt, and SciPy 1.0 Contributors. SciPy 1.0: Fundamental Algorithms for Scientific Computing in Python. *Nat. Methods*, 17:261–272, 2020. doi:10.1038/s41592-019-0686-2.
- Z. T. Wilson and N. V. Sahinidis. The ALAMO approach to machine learning. *Comput Chem Eng.*, 106:785–795, November 2017. doi:10.1016/j.compchemeng.2017.02.010.
- G. Wu, M. Á. de Carvalho Servia, and M. Mowbray. Distributional reinforcement learning for inventory management in multi-echelon supply chains. *Digital Chemical Engineering*, 6:100073, March 2023. doi:10.1016/j.dche.2022.100073.
- D. Zhang, E. A. del Rio-Chanona, P. Petsagkourakis, and J. Wagner. Hybrid physics-based and data-driven modeling for bioprocess online simulation and optimization. *Biotechnol. Bioeng.*, 116(11):2919–2930, July 2019. doi:10.1002/bit.27120.
- D. Zhang, T. R. Savage, and B. A. Cho. Combining model structure identification and hybrid modelling for photo-production process predictive simulation and optimisation. *Biotechnol. Bioeng.*, 117(11):3356–3367, July 2020. doi:10.1002/bit.27512.